JJEE
Volume 5, Number 4, 2019
Pages 244-266
Jordan Journal of Electrical Engineering
ISSN (Print): 2409-9600, ISSN (Online): 2409-9619

A Simulation Model for Analyzing Symmetrical Performance and Starting Methods in Three Phase Induction Motors

Omar M. Al-Barbarawi*

Electrical Engineering Department, Al Balqa' Applied University, Al Balqa', Jordan
E-mail: omaralbarbarawi@yahoo.com

Received: February 13, 2019 *Revised: March 15, 2019* *Accepted: April 6, 2019*

***Abstract*—** A mathematical model for a three-phase induction motor was developed using d-q axis theory. Investigations were carried out using MATLAB/SIMULINK for steady-state, as well as transient conditions when the motor is supplied from balanced and unbalanced voltage sources. Furthermore, soft and smooth starting of 3-phase induction motor was studied and analyzed through the proper choice of the firing angle (α) of thyristors over the starting period to control the applied voltage. The simulation results were analyzed for three induction motors with different power ratings: 3 hp, 50 hp and 500 hp. The results showed that the soft starting method has the lowest current magnitude, thus eliminating shaft-torque pulsations during the starting process and ensuring smooth build-up of torque and speed. It was also shown that increasing the firing angle caused torque and current magnitudes to increase faster, but at the same time it caused the motor to reach the steady-state faster.

***Keywords*—** Induction motor; Mathematical modeling; Starting methods; Balanced voltages; Torque-speed characteristic; Reference frame; Firing angle.

1. INTRODUCTION

The induction motors (IM) are widely used in industrial applications. Among its properties are self-static stability with a load variation and the ability to self-start [1-5]. Induction motors have been developed as constant-speed motors. However, with the progress of power electronics, induction motors have become able to operate as variable-speed motors [2]. An IM is considered a nonlinear dynamic system. Studying and analyzing dynamic behavior, steady-state operation and starting methods are very important in order to take changes in IM proceeding regime into account [3, 4]. It is important to calculate the mechanical transient cases during the starting process, since they cause high instantaneous currents to flow in the motor windings. As a result of these currents, mutual magnetic fluxes arise, producing electromagnetic torque, where the producing torque is proportional to the square of the starting current. Torque and currents can be adjusted by reducing the voltage during the starting process of the motor [15, 16]. The dynamic-mechanical characteristics of the motor depend on winding parameters, the hp of the motor and the value of rotor resistance, whereas the static (load) characteristics depend on load variations [5]. As a result, any change in these parameters leads to a change in the dynamic-mechanical characteristics [1, 3, 5].

Improvements in power semiconductor devices and fast digital signal processing hardware have contributed to accelerate the progress of studying and investigating the dynamic behavior of induction motors [4-6]. In this paper, a mathematical model is developed to study and analyze the behavior of induction motors; and the model is

* Corresponding author

simulated by using MATLAB/Simulink. The simulated mathematical model is based on the d-q axis theory in stationary reference frame and a synchronously rotating reference frame to analyze the dynamic-static performance of 3-phase IM during a normal operation and the starting process. The d-q axis theory is the most appropriate approach to calculate steady-state performance, starting process, electromagnetic torque-speed characteristics and stator currents of an IM [8-10]. Simulation has been carried out to investigate the behavior of three induction motors with power ratings of 3 hp, 5 hp, and 500 hp.

2. INDUCTION MOTOR MODELING

In order to study and analyze the transient cases and determine the behavior cases of the IM, we use the dynamic differential Eqs. (5) and (6) and the equivalent circuit shown in Fig. 1, which describe the motor performance in any of the transient cases. In this work non-linear differential equations are used to simulate the proposed model using MATLAB/Simulink. The model has been developed and built systematically by means of basic function blocks [1-5]. It uses d-q variables in asynchronously rotating reference frame. It is used to study the dynamic performance of the IM when it is supplied from a balanced voltage source in the starting process or in any transient case. When currents flow in the stator and rotor windings, electromagnetic transient cases arise. The balanced set of three-phase voltages can be represented as:

$$\begin{aligned} Va &= Vm\,sin(wt) \\ \mathrm{Vb} &= \mathrm{Vm}\sin(\mathrm{wt} - \pi/3) \\ \mathrm{Vc} &= \mathrm{Vm}\sin(\mathrm{wt} - 2\pi/3) \end{aligned} \tag{1}$$

In order to convert the 3-phase voltage into a 2-phase synchronously rotating frame, it is first converted into a 2-phase stationary frame (α, β) using:

$$\begin{pmatrix} \mathrm{V}\alpha \\ \mathrm{V}\beta \end{pmatrix} = \frac{2}{3}\begin{pmatrix} 1 & \frac{1}{2} & \frac{-1}{2} \\ 0 & \frac{\sqrt{3}}{2} & \frac{-\sqrt{3}}{2} \end{pmatrix}\begin{pmatrix} \mathrm{Va} \\ \mathrm{Vb} \\ \mathrm{Vc} \end{pmatrix} \tag{2}$$

Then, it is converted from a stationary frame into a synchronously rotating frame (d-q) using:

$$\begin{pmatrix} \mathrm{Vd} \\ \mathrm{Vq} \end{pmatrix} = \begin{pmatrix} \mathrm{Cos}\gamma & \mathrm{Sin}\gamma \\ -\mathrm{Sin}\gamma & \mathrm{Cos}\gamma \end{pmatrix}\begin{pmatrix} \mathrm{V}\alpha \\ \mathrm{V}\beta \end{pmatrix} \tag{3}$$

where (γ) is the transformation angle.

The conversion from a 2-phase frame into a 3-phase frame (dq–abc) is oppositely carried out by using Eqs. (4) and (5) as shown below:

$$\begin{pmatrix} \mathrm{i}\alpha \\ \mathrm{i}\beta \end{pmatrix} = \begin{pmatrix} \mathrm{Cos}\gamma & \mathrm{Sin}\gamma \\ -\mathrm{Sin}\gamma & \mathrm{Cos}\gamma \end{pmatrix}\begin{pmatrix} \mathrm{id} \\ \mathrm{iq} \end{pmatrix} \tag{4}$$

$$\begin{pmatrix} \mathrm{ia} \\ \mathrm{ib} \\ \mathrm{ic} \end{pmatrix} = \begin{pmatrix} 1 & 0 \\ \frac{1}{2} & \frac{\sqrt{3}}{2} \\ \frac{-1}{2} & \frac{-\sqrt{3}}{2} \end{pmatrix}\begin{pmatrix} \mathrm{i}\alpha \\ \mathrm{i}\beta \end{pmatrix} \tag{5}$$

The dynamic equations are:

$$\tilde{V}s = Rs\boldsymbol{i}s+\frac{d\Psi s}{dt} + \omega e\, \Psi s \tag{6}$$

and

$$\tilde{V}r = Rr\boldsymbol{i}r\frac{d\Psi_r}{dt} + (\omega e - \omega r)\Psi r \tag{7}$$

Flux linkage and current can be expressed as:

$$\Psi = \begin{pmatrix}\Psi s\\ \Psi r\end{pmatrix} \quad ; \qquad \boldsymbol{i} = \begin{pmatrix}id\\ iq\end{pmatrix} \tag{8}$$

Flux linkage expressions can be written in terms of currents as follows:

$$\Psi s = Ls\boldsymbol{i}s + Lm\boldsymbol{i}r \qquad , \qquad \Psi r = Lr\boldsymbol{i}r + Lm\boldsymbol{i}s \tag{9}$$

where

$$Ls = Lm + L_{ls} \quad \text{and} \quad Lr = Lm + L_{lr} \tag{10}$$

By substituting Eq. (10) in Eq. (9) and multiplying it by (ω_b), flux linkage and mutual flux expressions in terms of currents can be written as follows:

$$F_{ds} = \omega_b\Psi_{ds} = \omega_b[L_{ls}i_{ds} + L_m(i_{ds} + i_{dr})]$$

$$F_{qs} = \omega_b\Psi_{qs} = \omega_b[L_{ls}i_{qs} + L_m(i_{qs} + i_{qr})] \tag{11}$$

$$F_{dr} = \omega_b\Psi_{dr} = \omega_b[L_{lr}i_{dr} + L_m(i_{ds} + i_{dr})\,]$$

$$F_{qr} = \omega_b\Psi_{qr} = \omega_b[L_{lr}i_{qr} + L_m(i_{qs} + i_{qr})] \tag{12}$$

$$F_{dm} = \omega_b\Psi_{dm} = \omega_b[L_m(i_{ds} + i_{dr})]$$

$$F_{qm} = \omega_b\Psi_{qm} = \omega_b[L_m(i_{qs} + i_{qr})] \tag{13}$$

In the stationary reference frame, stator and rotor currents (i_{ds} , i_{dr}) can be expressed in terms of flux linkages as follows:

$$i_{ds} = (F_{ds} - F_{dm})/\omega_b L_{ls} \quad i_{qs} = (F_{qs} - F_{qm})/\omega_b L_{ls} \tag{14}$$

$$i_{dr} = (F_{dr} - F_{dm})/\omega_b L_{lr}\, i_{qr} = (F_{qr} - F_{qm})/\omega_b L_{lr} \tag{15}$$

By converting Eqs. (6) and (7) into synchronously rotating d-q axes, and substituting the relationship $[\Psi_{(s,r)} = F_{(s,r)}/\omega_b]$ in these equations, the stator and rotor voltages as well as the flux linkages equations for dynamic simulation are obtained as follows:

$$V_{qs} = R_s i_{qs} + \frac{\omega_e}{\omega_b}F_{ds} + \frac{1}{\omega_b}\frac{dF_{qs}}{dt}V_{ds} = R_s i_{ds} - \frac{\omega_e}{\omega_b}F_{qs} + \frac{1}{\omega_b}\frac{dF_{ds}}{dt} \tag{16}$$

$$V_{qr} = R_r i_{qr} + \frac{\omega_e - \omega_r}{\omega_b}F_{dr} + \frac{1}{\omega_b}\frac{dF_{qr}}{dt}V_{dr} = R_r i_{qr} - \frac{\omega_e - \omega_r}{\omega_b}F_{dr} + \frac{1}{\omega_b}\frac{dF_{dr}}{dt} \tag{17}$$

$$\frac{dF_{qr}}{dt} = \omega_e\left[V_{qs} - \frac{\omega_e}{\omega_b}F_{ds} + \frac{R_s}{X_{ls}}(F_{mq} - F_{qs})\right]\frac{dF_{qr}}{dt} = \omega_e\left[V_{ds} + \frac{\omega_e}{\omega_b}F_{ds} + \frac{R_s}{X_{ls}}(F_{md} - F_{qs})\right] \tag{18}$$

$$\frac{dF_{qr}}{dt} = \omega_e \left[-\frac{\omega_e - \omega_r}{\omega_b} F_{dr} + \frac{R_r}{X_{lr}} \left(F_{mq} - F_{qr} \right) \right] \frac{dF_{dr}}{dt} = \omega_e \left[\frac{\omega_e - \omega_r}{\omega_b} F_{qs} + \frac{R_s}{X_{ls}} \left(F_{md} - F_{dr} \right) \right] \quad (19)$$

Mutual fluxes are given as follows:

$$F_{mq} = X_{lm} \left[F_{qs}/X_{ls} + F_{qr}/X_{lr} \right] F_{md} = X_{lm} \left[F_{ds}/X_{ls} + F_{dr}/X_{lr} \right] \quad (20)$$

where:

$$X_{lm} = \frac{X_{m.} X_{ls} X_{lr}}{X_{ls} X_{lr} + X_{m.} X_{lr} + X_{m.} X_{ls}} \text{ and } X_{ls} = \omega_b L_{ls} \quad , X_{lr} = \omega_b L_{lr} \quad , \; X_m = \omega_b L_m$$

After finding flux linkages and currents, the electromagnetic torque can be calculated:

$$T_{em} = \frac{3}{4} \frac{1}{\omega_e} P \left(F_{ds} i_{qs} - F_{qs} i_{ds} \right) \quad (21)$$

when the torque is found, the motor speed can be calculated using:

$$T_{em} - T_{load} = \frac{2J}{P} \frac{d\omega_e}{dt} \quad (22)$$

where $\omega_b = 2\pi f$ is the machine's base frequency; ω_e is the synchronous speed at which the rotating frame rotates; ω_r is the real angular speed of the rotor. The d-q axes are fixed on the rotor moving at a speed of $(\omega_e - \omega_r)$ relative to a synchronously rotating frame. $\tilde{V}_s$ and $\tilde{V}_r$ are the voltage space vectors of the stator and rotor, respectively. i_{ds} and i_{dr} represent the current space vectors of the stator and rotor, respectively. F_d and F_q are the flux linkage space vectors of the stator and rotor, respectively. While Ψ_d and Ψ_q are the flux linkages of the stator and rotor, *i*s and *i*r are the stator and rotor currents. R_s and R_r are the resistances of the stator and rotor, respectively. X_{ls} , X_{lr} and X_m are the stator leakage reactance, the rotor leakage reactance, and magnetizing reactance, respectively. L_s and L_r are the stator and rotor inductances. L_{ls} and L_{lr} are the stator and rotor leakage inductances. L_m is the magnetization inductance .T_{em} is the electromagnetic torque; and T_L is the load torque. P is the number of poles. i_α and i_β are the stator and rotor currents in the α, β frame. ω_e is the angular speed of the reference frame. J is the moment of inertia. V_α and V_β are the stator and rotor voltages in the α, β frame.

3. SIMULINK MODEL OF 3-PHASE INDUCTION MOTOR

A mathematical model is built to study the dynamic behavior of an induction motor in the d-q axes. The model consists of a number of sub-blocks: a) 3-phase voltage source; b) abc-dq axes sub-block which realizes the transformation of variables defined by Eqs. (2) and (3); c) dq-abc voltage conversion sub-block as defined by Eqs. (4) and (5); d) calculations sub-block of motor constants and coefficients, variable voltage parameters, electromagnetic torque and load torque defined by Eq. (13). Fig. 1 shows the dynamic equivalent circuit, while Fig. 2 illustrates a block diagram of a 3-phase induction motor.

Fig. 3 shows the induction motor d-q model, which represents the induction motor using d-q axes in an arbitrary reference frame. This model consists of two main parts: the electrical model and the dynamical model as depicted in Eqs. (11-20).

Fig. 4 illustrates the complete block diagram for finding the flux linkages and mutual fluxes in d- q- axis in an arbitrary reference frame. Fig. 5 shows the sub-blocks diagram of flux linkages. Fig. 6 shows the sub-block diagram of mutual fluxes (Fmq and Fmd) which are calculated using Eq. (20). Fig. 7 shows the complete block diagram for finding the currents in d-q axis whereas Fig. 8 illustrates the sub-block- diagram for finding ($\boldsymbol{i}_{qs}$, $\boldsymbol{i}_{ds}$, $\boldsymbol{i}_{qr}$, and $\boldsymbol{i}_{dr}$). Fig. 9 shows the mechanical system block diagrams which determine the electromagnetic torque basing on Eq. (21) and the speed of the motor using Eq. (22). Three motors with power ratings of 3 hp, 50 hp, and 500 hp will be used for simulation in normal cases with a balanced voltage operation and starting method operation. The parameters of these motors are summarized in Table 1.

Table 1. Induction machine parameters.

hp	Volt	RPM	TB [N.m]	IB [A]	RS [PU]	R'R [PU]	L1S [PU]	L'1R [PU]	LM [PU]	J [Kg.m2]	H
3	220	1425	14.07	5.8	0.0199	0.0373	0.0373	0.0344	1.193	0.089	0.497
50	460	1421	237.38	46.8	0.0153	0.0402	0.0532	0.0532	2.305	1.662	0.477
500	2300	1485	10.6810[2]	93.6	0.0185	0.0132	0.085	0.085	3.808	11.05	0.369

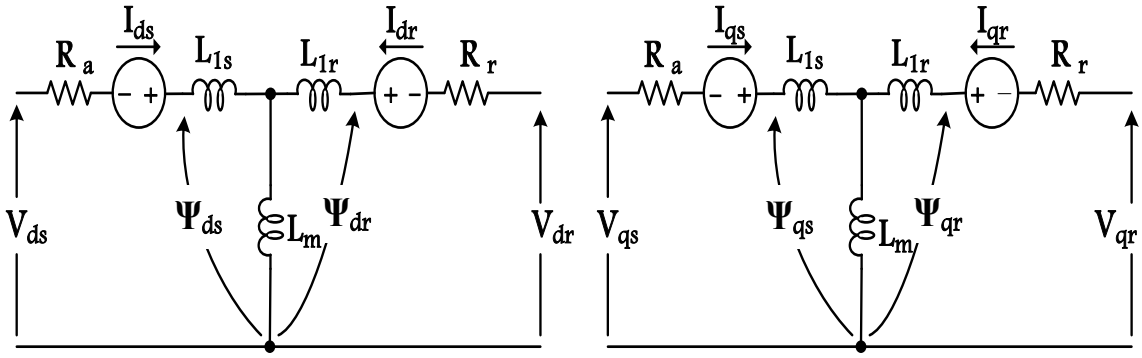

Fig. 1. d-q dynamic equivalent circuit.

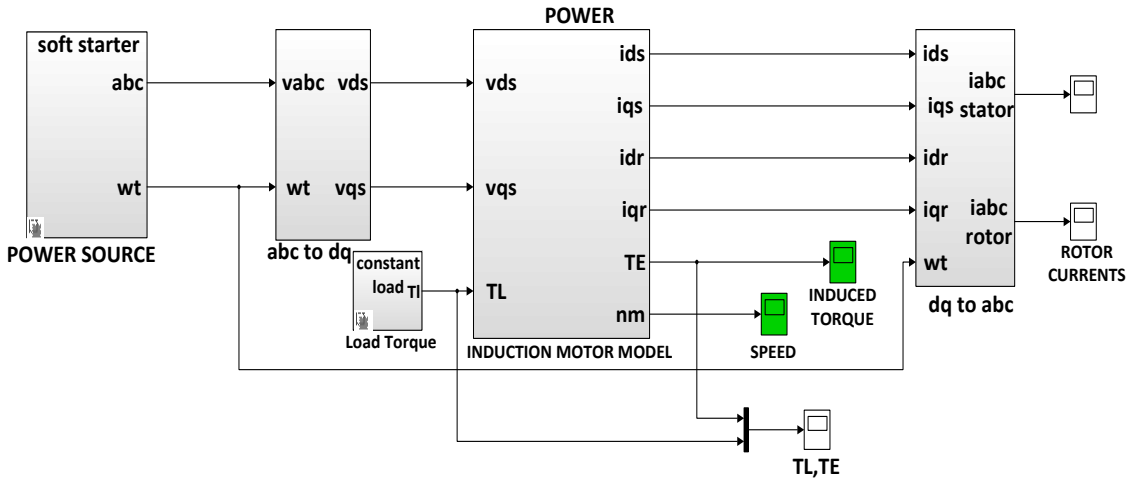

Fig. 2. Block diagram of a three phase induction motor.

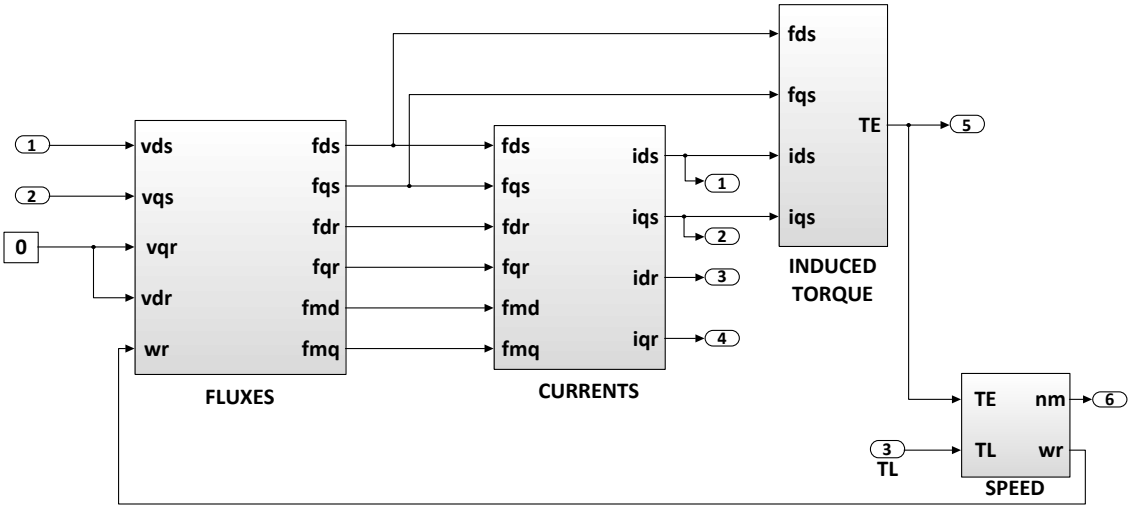

Fig. 3. Block diagram of a 3-phase induction motor with flux Linkage-current relations in d-q - axis in an arbitrary reference frame.

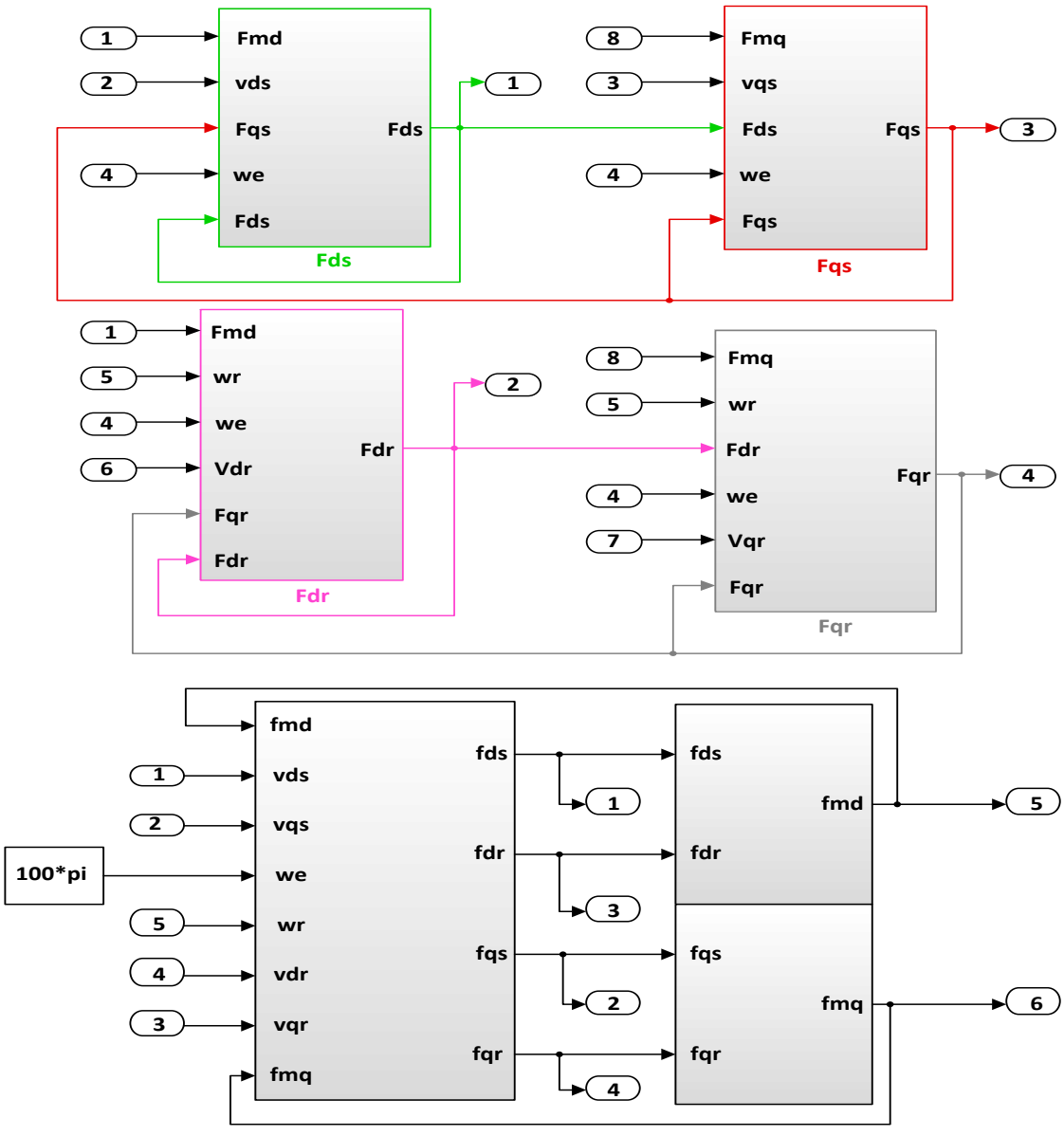

Fig. 4. Complete block diagram for finding flux linkages and mutual fluxes in d-q-axis.

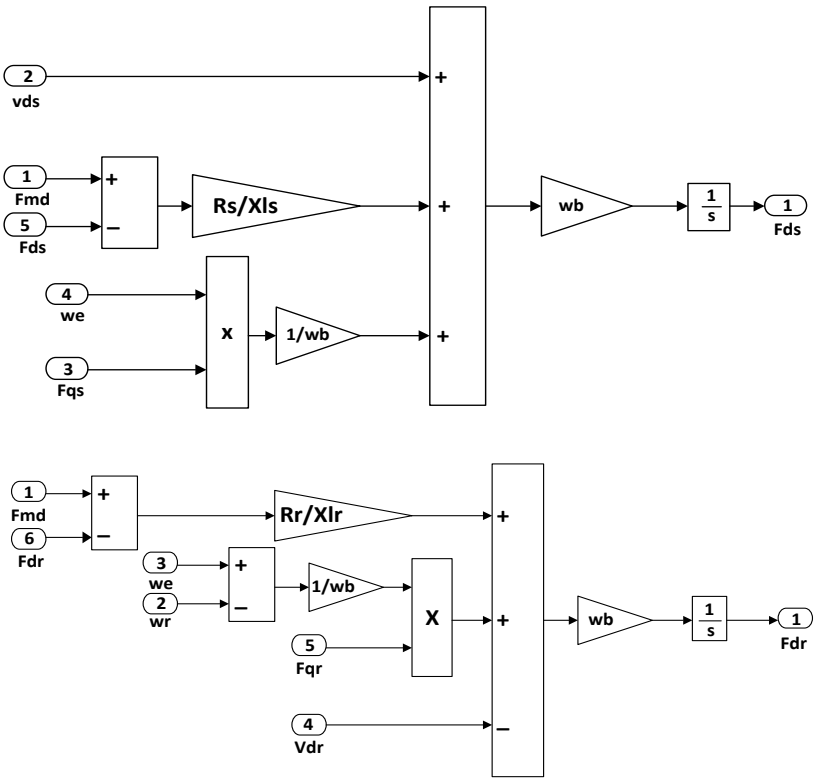

Fig. 5. Sub-block diagram for finding flux linkages (Fqs, Fds, Fqr and Fdr).

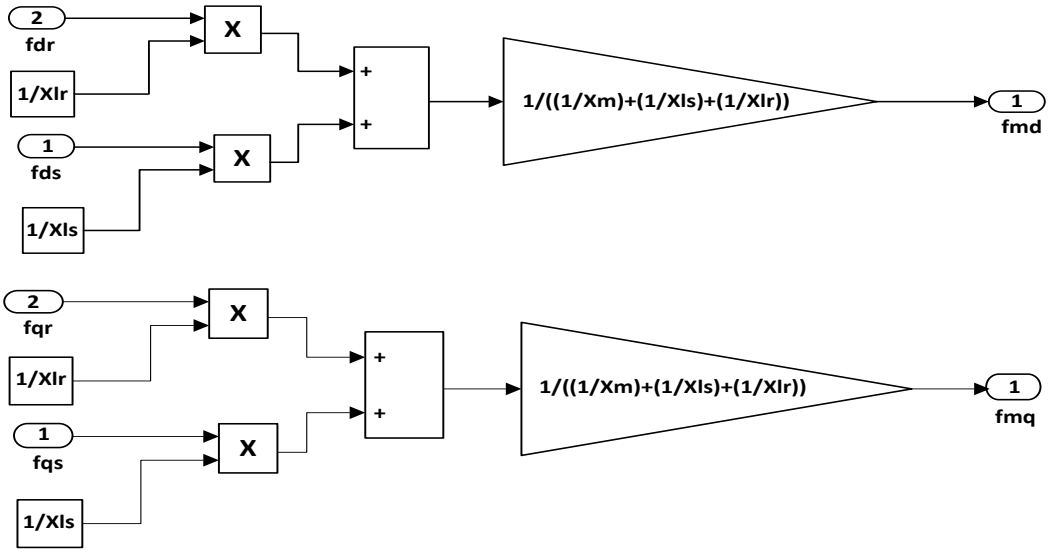

Fig. 6. Sub-block diagram for finding mutual flux linkages (Fmq and Fmd).

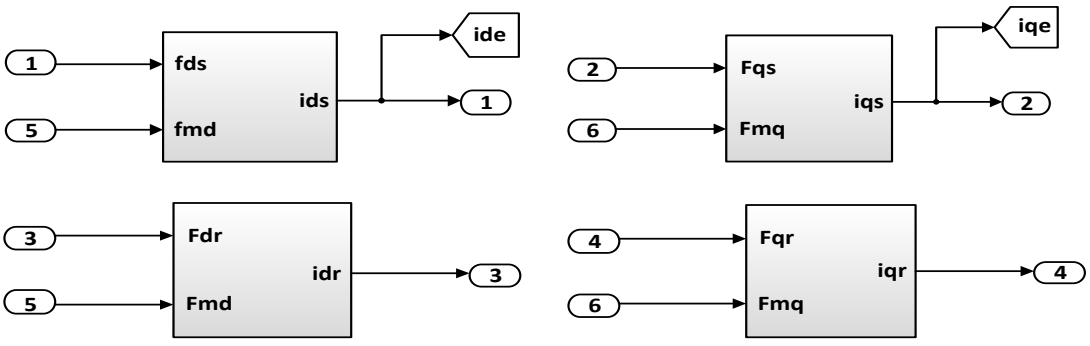

Fig. 7. Complete block diagram for finding currents in d-q axis.

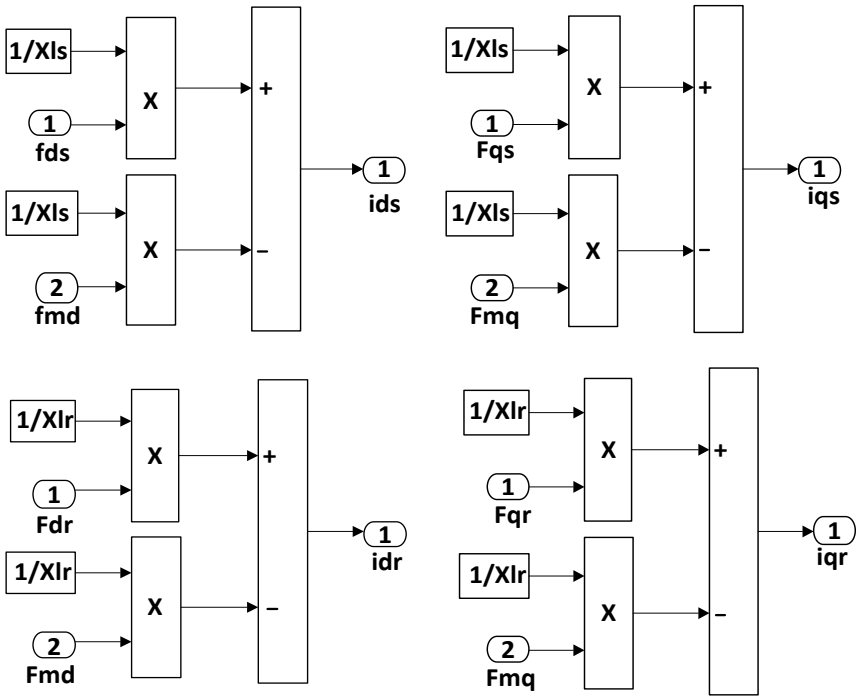

Fig. 8. Sub-block diagram for finding ($\boldsymbol{i}_{qs}$, $\boldsymbol{i}_{ds}$, $\boldsymbol{i}_{qr}$, and $\boldsymbol{i}_{dr}$).

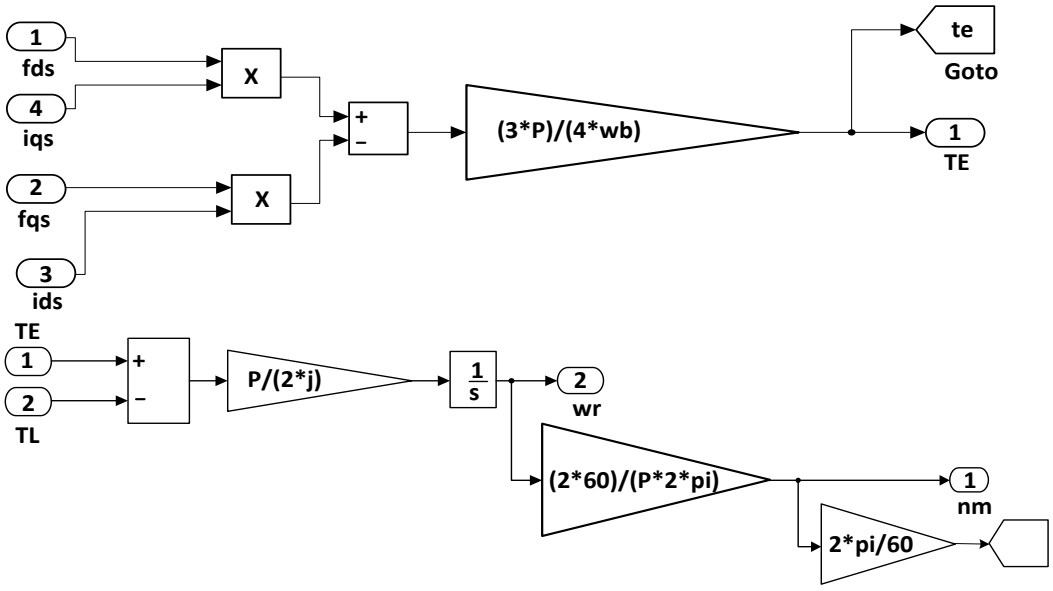

Fig. 9. Block diagram for finding the electromagnetic torque and speed.

4. RESULTS OF INDUCTION MOTOR SIMULATION

Three motors with different power ratings and different parameters are simulated. The three motors are simulated under no-load condition using direct on-line starting: The electromagnetic torque characteristic can be expressed during normal operations through the relationship between the electromagnetic torque and motor speed or slip as shown in the figures below. The results of studying the IM dynamic behavior using MATLAB/Simulink illustrate the effect of transient cases such as starting the motor. Electromagnetic torque and currents flowing in the windings of the stator and rotor appear in a form of cartographic curves as a function of time or speed

with a large strike (in-rush) current that arises with a few cycles. More oscillations and high peak values appear as a result of the high instantaneous input current drawn by a motor during the initial starting process, where the induction motor behaves as a transformer with a short-circuited rotor until it begins to rotate. Currents flowing in the motor's windings during transient cases such as the starting process contain two components; a DC component and AC component. These are formed as a result of I'-sub transient, I'-transient and I-steady state currents which correspond to the reactance values. The DC component will fade to zero at the end of an electromagnetic transient case depending on the winding time constant. Analyzing the effect of the motor parameters in transient cases gives a perception of the quality and characteristic of transient cases and situations for defining the peak value of the torque, strike current and transient process period. From the simulation results, one can observe that at the instant when the motor begins to rotate, a large strike (in-rush) current as well as oscillation current arises in the stator. Fig. 10 shows the dynamic voltage conversion signals (V_abc, V_αβ, and V_dq) of both the 50 hp and 500 hp simulated motors supplied by a balanced voltage source.

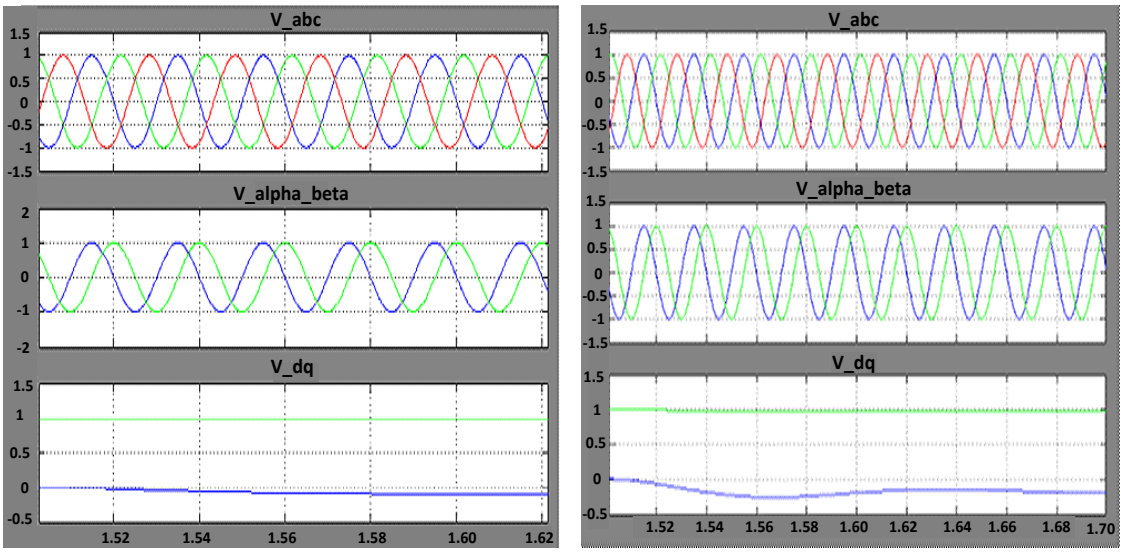

Fig. 10. Dynamic performance of voltage conversion signals (V_abc, V_αβ, V_dq) for: a) 50 hp/ 460V; b) 500 hp/2300V induction motors supplied by a balanced voltage source.

Fig. 11 illustrates the behavior of motor and oscillatory currents during start-up and normal operation at no-load condition. Strike currents value increases dramatically to reach a peak of about 14 PU during one cycle with a few numbers of current oscillations having a peak of about 13.5 PU for the 3 hp motor. In a 50 hp motor, the strike current increases to reach a peak of about 10.6 PU during one cycle with a few numbers of current oscillations having about 9.6 PU. For comparison , for the 500 hp motor , the strike current increases to reach a peak of about 9.5 PU during one cycle with a few number of current oscillations having a peak of about 6.6 PU. All oscillation currents will disappear when the motor reaches its rated speed. At the end of the transient case, the motor reaches the synchronous speed.

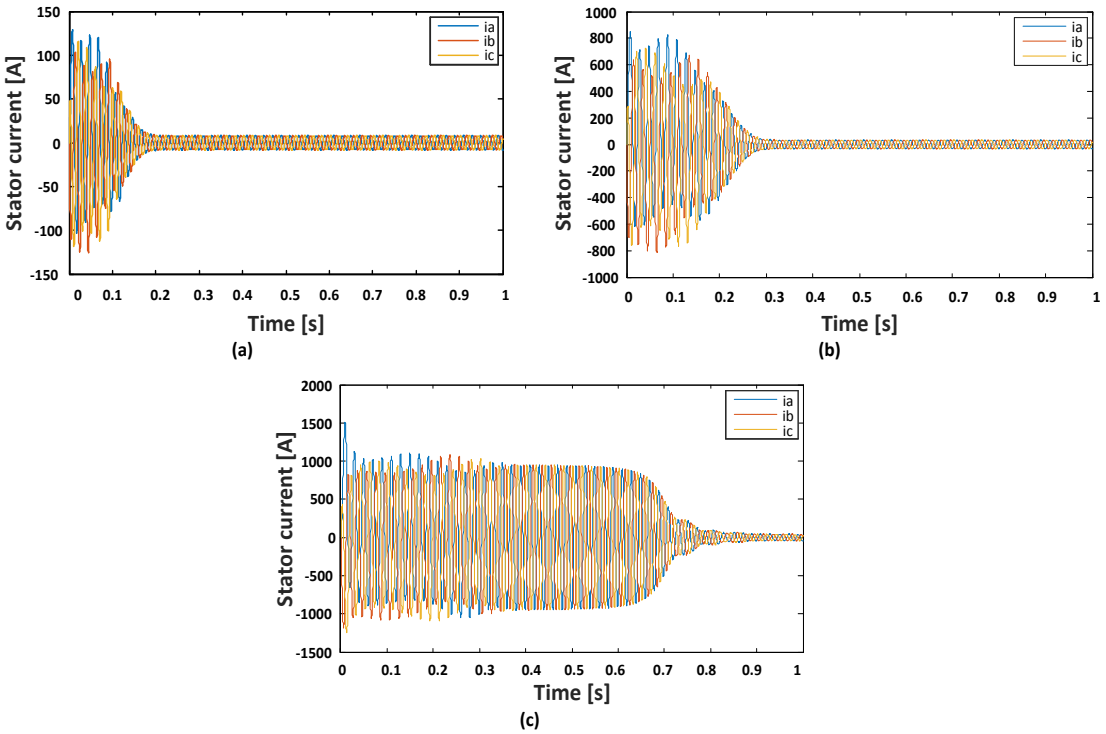

Fig. 11. Stator current signals for the induction motors: a) 3 hp; b) 50 hp; c) 500 hp.

By increasing the moment of inertia or the hp of the motor, the number of oscillations in the torque-speed characteristic value increases dramatically until a peak of about (-1.8 to 2.5) PU for a 500 hp motor, but the torque-speed oscillations disappears when the motor speed reaches 0.22 of the synchronous speed. For 3 hp and 50 hp motors, the number of oscillations increases dramatically until a peak of about (-1 to 12.35) PU and (-2.8 to 8.5) PU respectively. The oscillation will disappear when the motor speed reaches 0.53 and 0.48 of the synchronous speed as shown in Fig. 12.

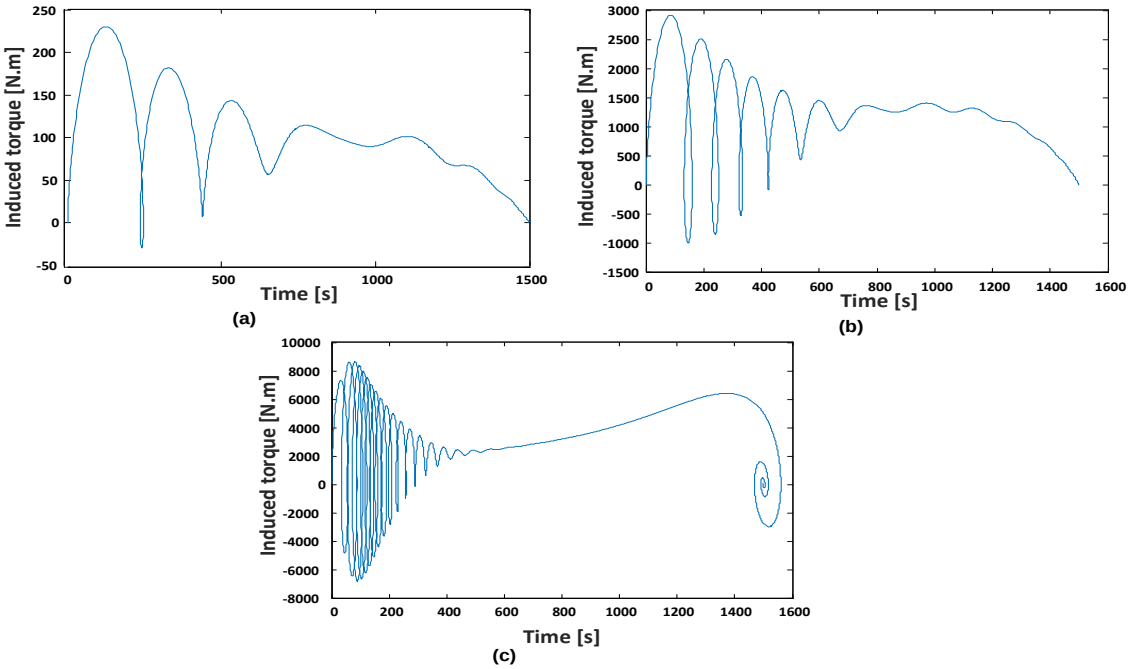

Fig. 12. Torque-speed characteristics for the induction motors: a) 3 hp; b) 50 hp; c) 500 hp.

Fig. 13 illustrates the torque of the 3 hp motor. The torque value increases dramatically to reach a peak of about (12.2) PU with a very few number of torque oscillations; and the motor reaches the steady state after about 0.3 s. For the 50 hp motor, the torque value increases to reach a peak of about (8.2) PU, with a few number of oscillations. The motor reaches the steady state after about 0.4 s. For the 500 hp motor, there are more torque oscillations; and the torque value increases until reaching a peak of about (2.5) PU. The 500 hp motor reached the steady state within about 1.3 s.

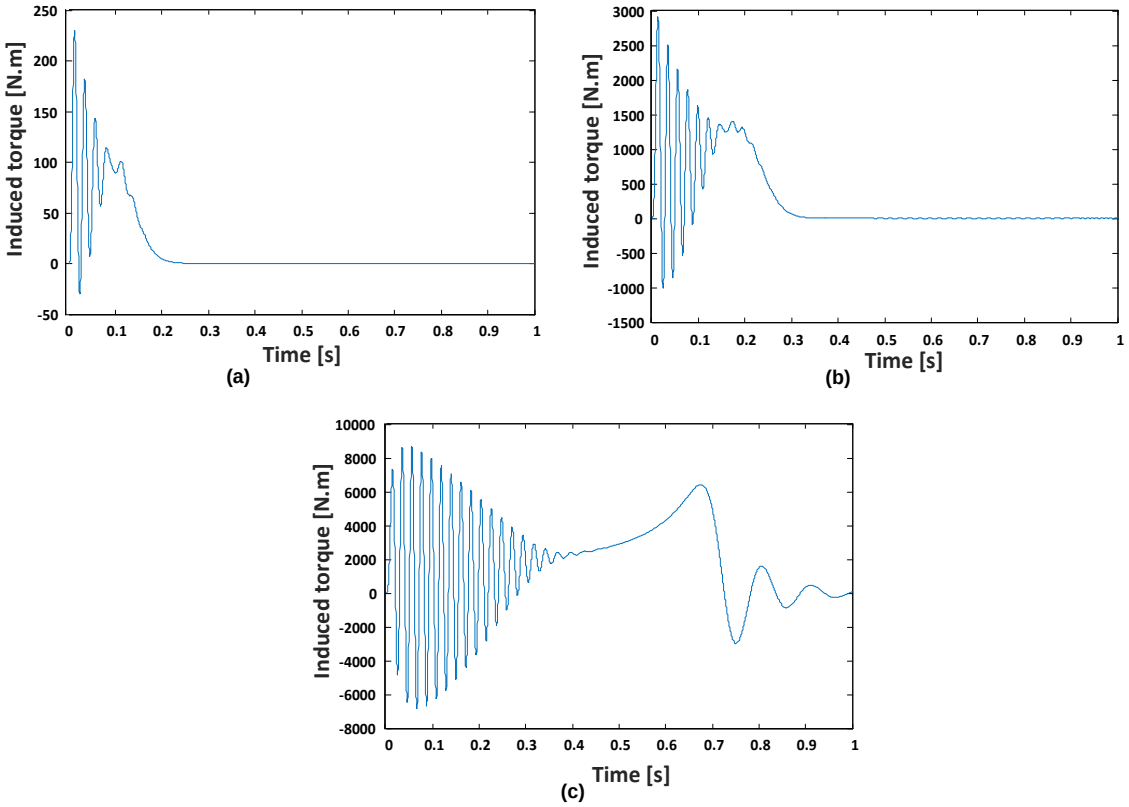

Fig. 13. Torque signal characteristic for the induction motors: a) 3 hp; b) 50 hp; c) 500 hp.

Fig. 14 illustrates the motor speed, where the motor accelerates up to reach the rated speed. They take less time (about 0.3 s) for motors lower power rating (3 hp and 50 hp), and more time (about 1.05 s) when the power rating is higher (500 hp). When the speed of the motor exceeds the synchronous speed, the stator current as well as the torque will not be equal to zero. The current flow direction is reversed, causing the torque to brake and reduce the motor speed to reach stability at the rated speed value.

5. STUDYING DIFFERENT STARTING METHODS

Here, we focus on simulating different starting methods under different loading conditions using a 50 hp/220 V induction motor. Each load condition will be simulated with different starting methods: Direct On-line Starting, Star-Delta starting, and soft starting. Four different loading conditions were simulated: 1) No Load; 2) Constant Load; 3) Step Load; and 4) Ramp Load.

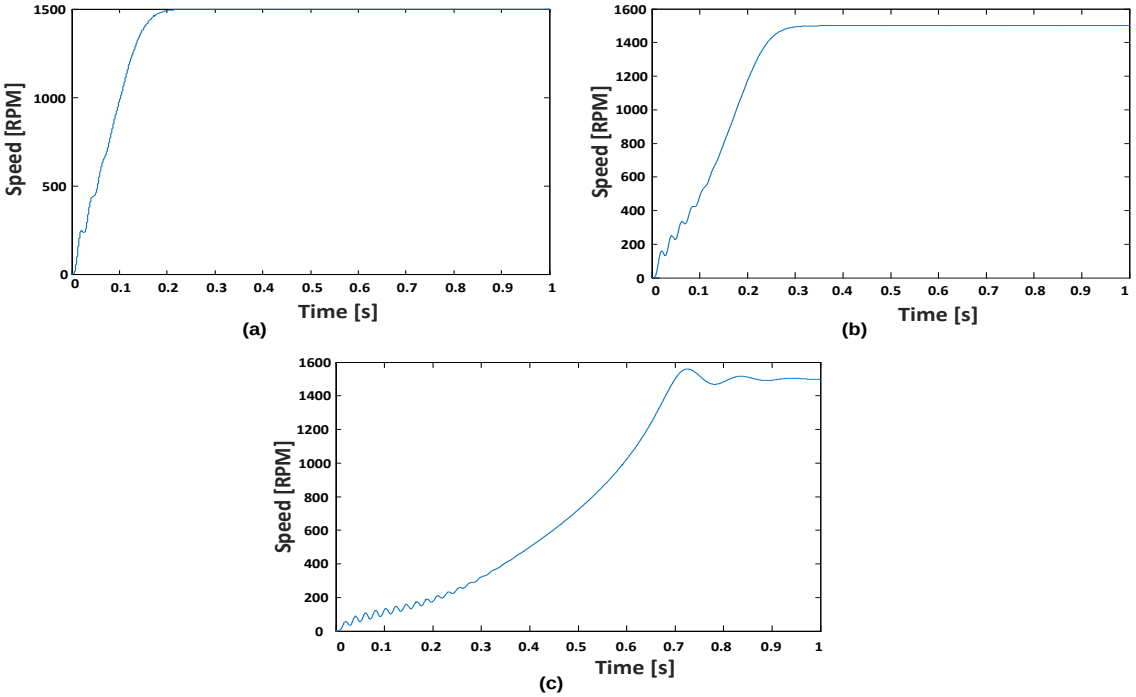

Fig. 14. Speed signal for the hp induction motors: a) 3 hp; b) 50 hp; c) 500.

5.1. No Load

5.1.1. Direct On-line Starting

In this method, the motors draw a large starting current. In order to reduce the starting current; induction motors are started by a reduced voltage using star- delta starting and soft starting. The simulation results are shown in Fig. 15 which illustrates the stator current, torque and speed vs. time, and torque-speed characteristics under no-load condition.

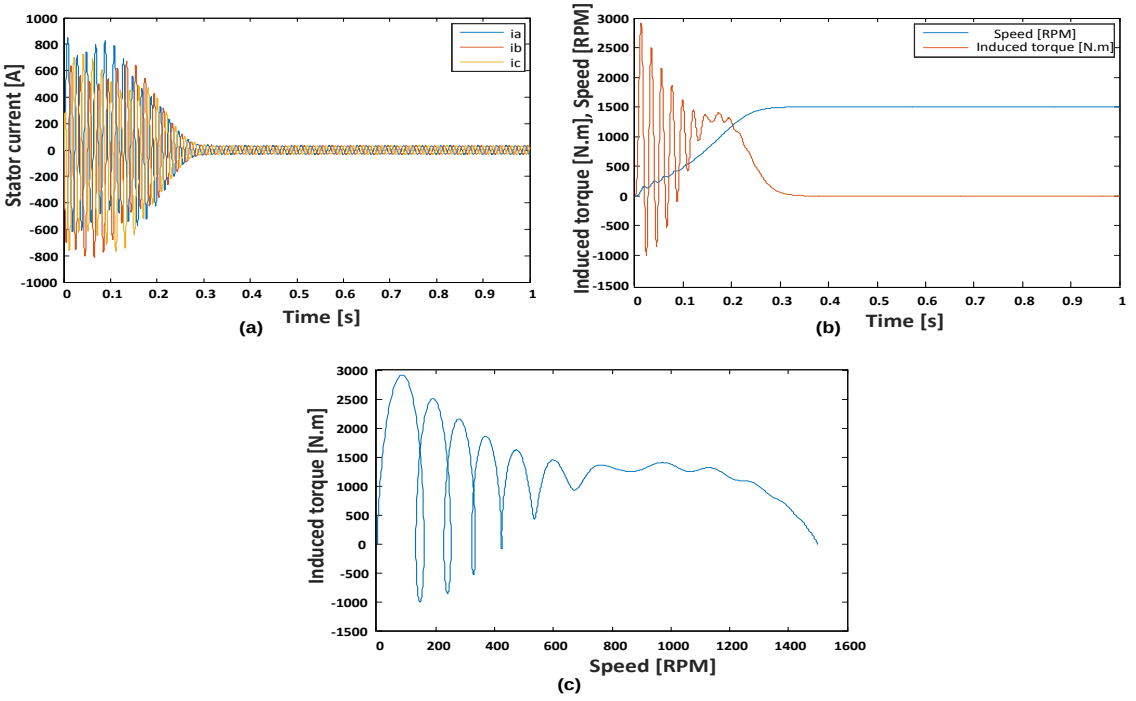

Fig. 15. a) Stator current; b) torque and speed vs. time; c) torque-speed characteristics.

5.1.2. Star-Delta Starting

Curves in Fig. 16 illustrate the stator current, torque and speed versus time, and torque-speed characteristics of the induction motor when using star-delta starting, where line current and the starting torque of the motor are reduced to one-third as compared to delta starting.

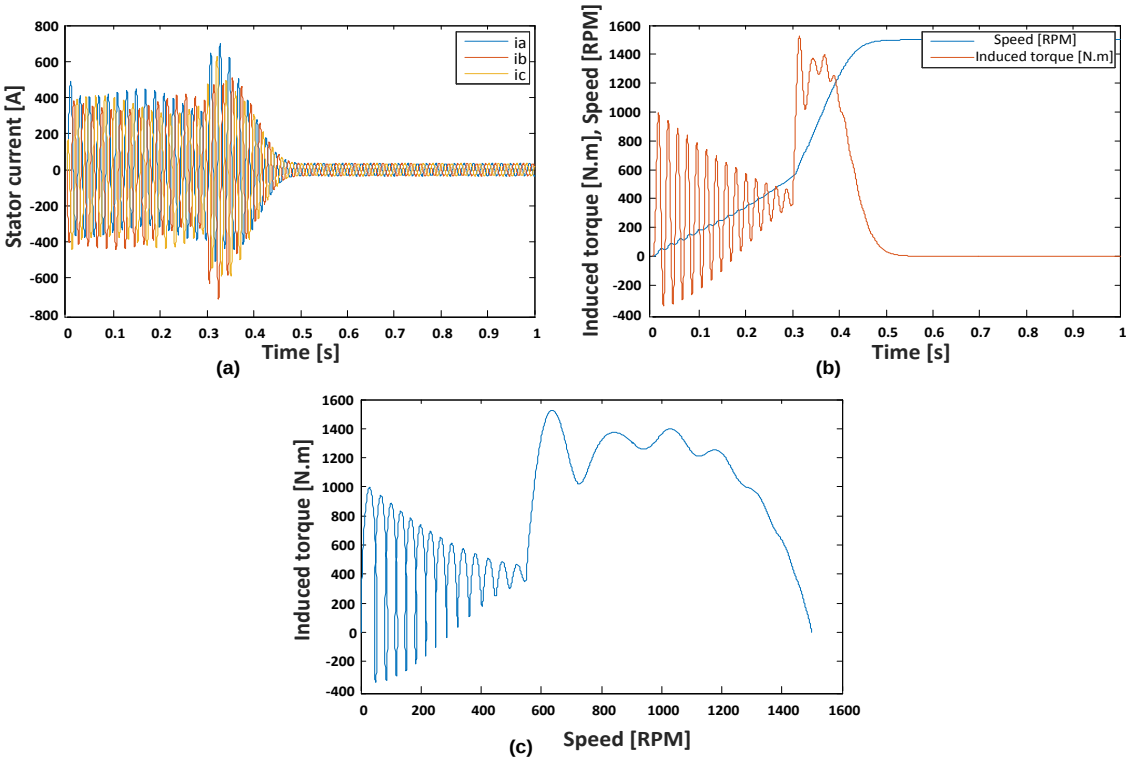

Fig. 16. a) Stator currents; b) torque and speed vs. time; c) torque-speed characteristics.

5.1.3. Soft Starting

At the time of starting, in case of on-line starting, a three phase induction motor draws a very high current with a low power factor. This current exceeds the motor capacity, leads to high electrical stresses on the motor windings and produces severe pulsations in the electromechanical torque, which may cause shocks to the driven equipment as well as damage to the mechanical system components. In order to remedy this disadvantageous effect, a common method is used by employing power semiconductors for current control. This starting method is known as soft starting of induction motor. Normally, soft starting is achieved by reducing the starting voltage. Using soft starting for induction motors controls the motor speed so that it increases gradually. This, in turn, protects the motor against mechanical shocks and electrical stress on the motor windings; and improves the performance of the induction motor as compared to direct starting. Load torque characteristics are also improved through the use of soft starting. A soft starter consists of six SCRs, each two of them are connected in an anti-parallel configuration in each phase [14-17]. In this paper, we study and analyze soft starting of induction motors using a controlled voltage. Based on the SCR, firing angle is triggered with a full-delay-firing angle during starting. Then, it gradually reduces the delay till it reaches zero. The SCR firing angle is controlled by a slope signal which generates a fixed-value 180^{o} degree ramp whereas the controller

generates another signal which is then compared with the ramp signal. This leads to reduce the voltage during starting which is then gradually built-up until reaching a full supply voltage. The reference signal value gradually increases, leading to eliminating the starting torque pulsations, so that the motor starts slowly and reaches its full rated speed gradually.

5.1.4. Simulation Results

Figs. 17-19 illustrate the simulation results on terms of three phase induction motor waveforms of voltage, current, torque, and speed when using soft starting at no-load with generating -180°, -360°, and -540° ramps respectively.

In case of (*-180*°) slope all parameters increase smoothly to reach the rated values in 0.45 s for voltage, and 0.85 s for current, speed and torque with limited oscillations as shown in Fig. 17.

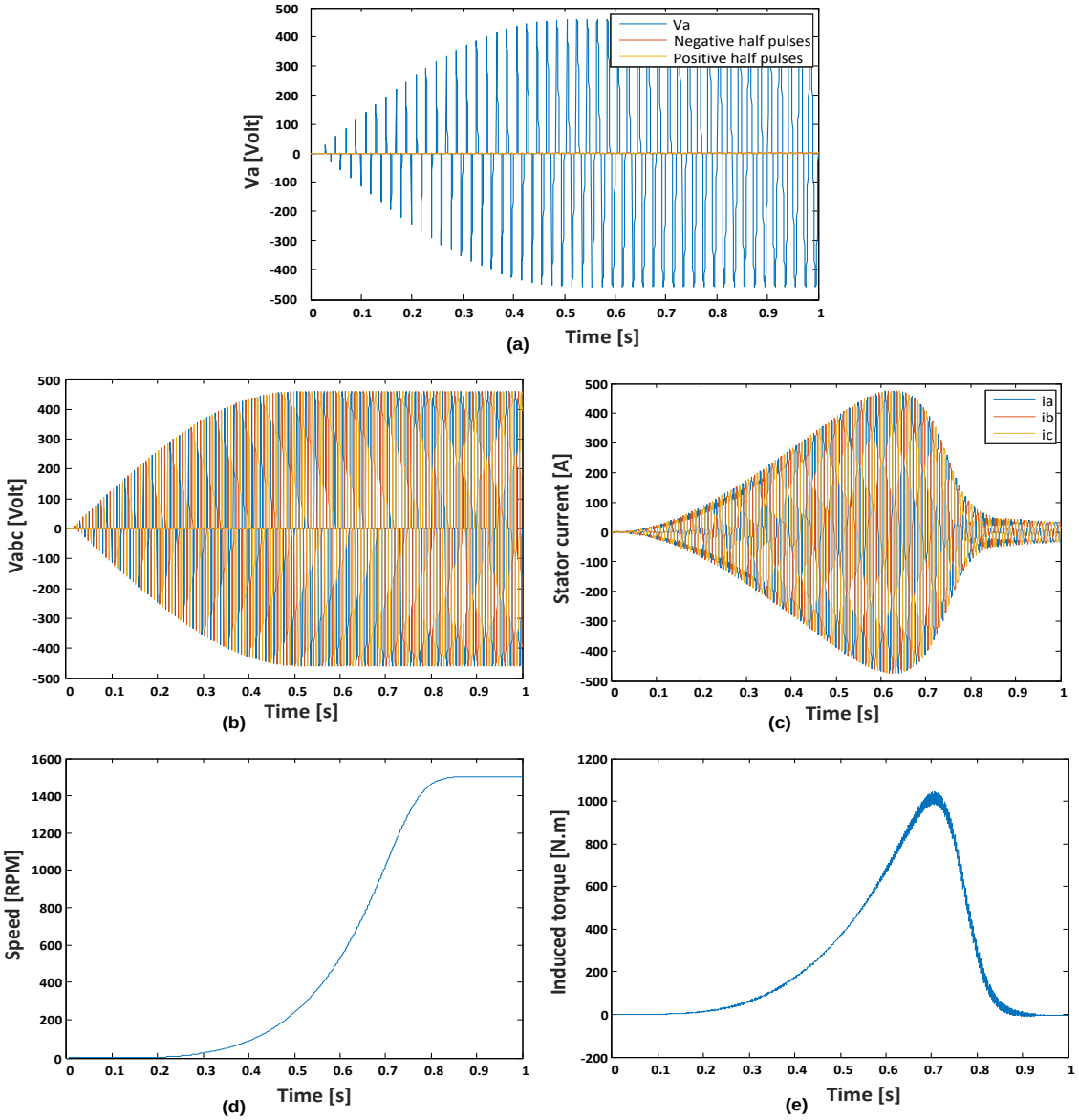

Fig. 17. a) Starting waveform voltage build-up with each phase; b) 3-phase voltages with initial firing angle= 180° with a slope of -180°; c) starting stator currents in the 3- phase; d) speed with a slope of -180°; f) torque characteristics.

For the (*-360°*) slope case, all parameters increase smoothly to reach the rated values in 0.3 s for voltage, and 0.52 s for current, speed and the torque with limited oscillations as shown in Fig. 18.

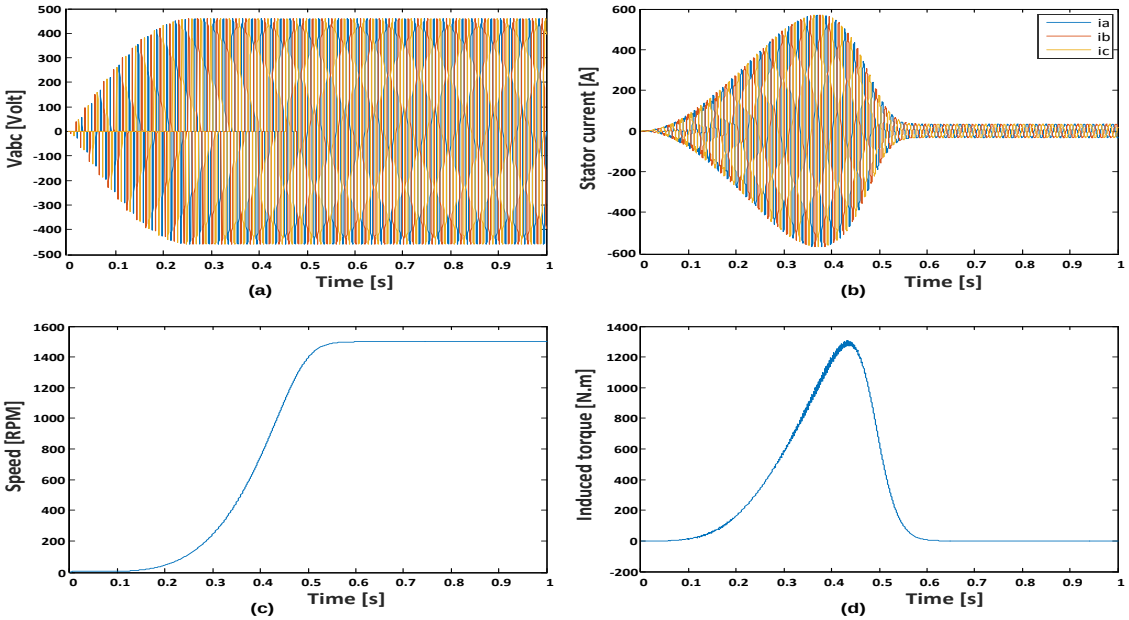

Fig. 18. a) 3-phase voltages with initial firing angle= 180° with a slope of -360°; b) starting stator currents in the 3- phase; c) speed with a slope of -360°; d) torque characteristics.

In case of (*-540°*) all parameters increase smoothly to reach the rated values through 0.15 s for voltage, and 0.42 s for starting current, speed and the torque with limited oscillations as shown in Fig. 19.

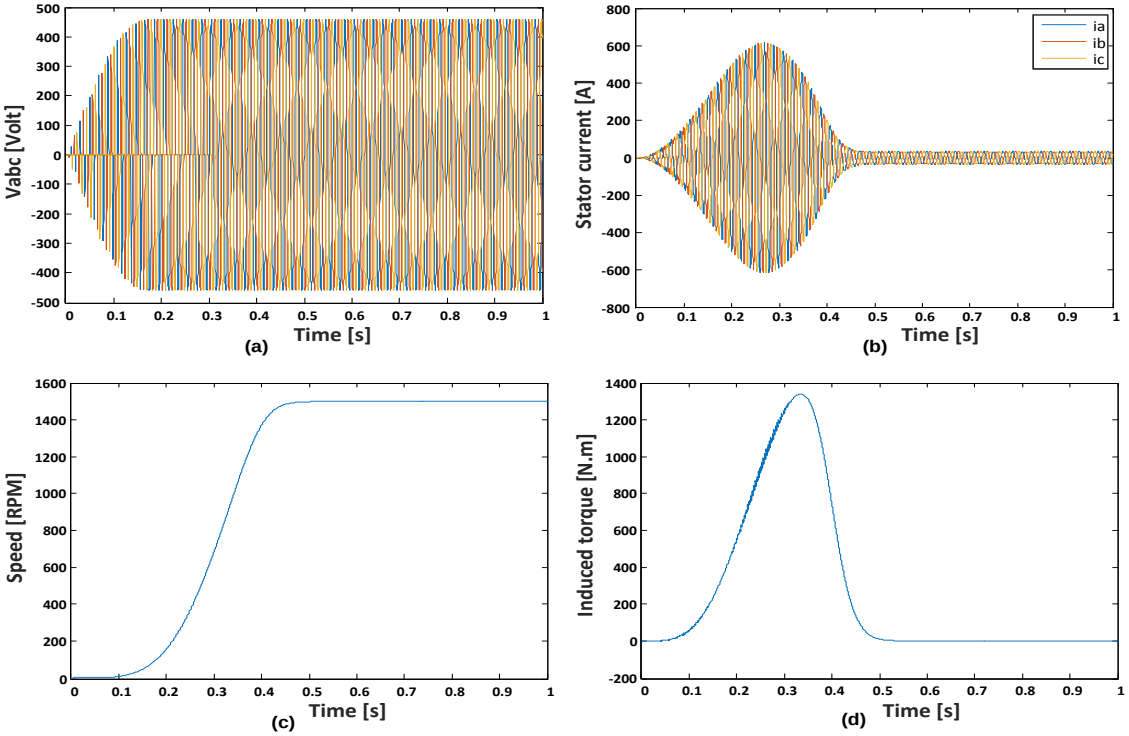

Fig. 19. a) Starting voltage build-up in the 3-phase; b) starting stator currents in the 3-phase; c) speed with a slope of -540°; d) torque characteristics.

Fig. 20 shows a comparison of the starting performance for the three slope values. Currents, speeds and torques are illustrated for slopes of -540°, -360°, and -180° respectively. It can be observed that the studied parameters are built up smoothly to reach the rated values over a longer period of time.

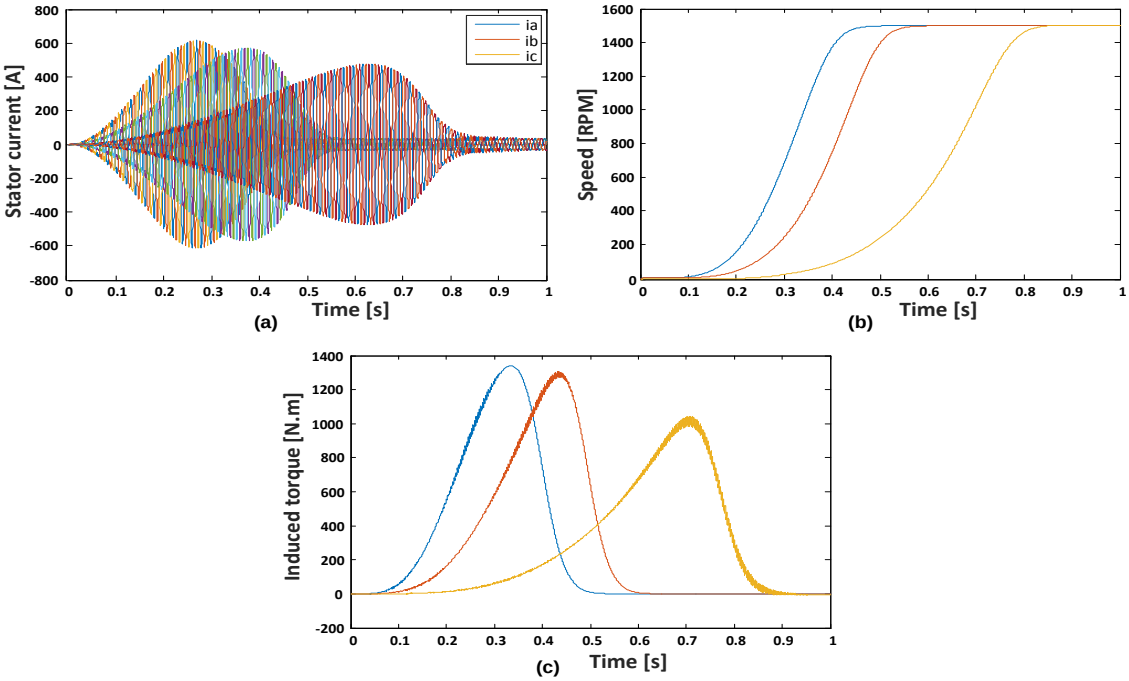

Fig. 20. a) Stator currents for slopes -540°, -360°, and -180° respectively; b) speed for slopes -540°, -360°, and -180° respectively; c) torque for slopes -540°, -360°, and -180° respectively.

5.2. Constant Load

5.2.1. Direct On-line Starting

Fig. 21 shows the simulation results of direct on-line starting at a constant load.

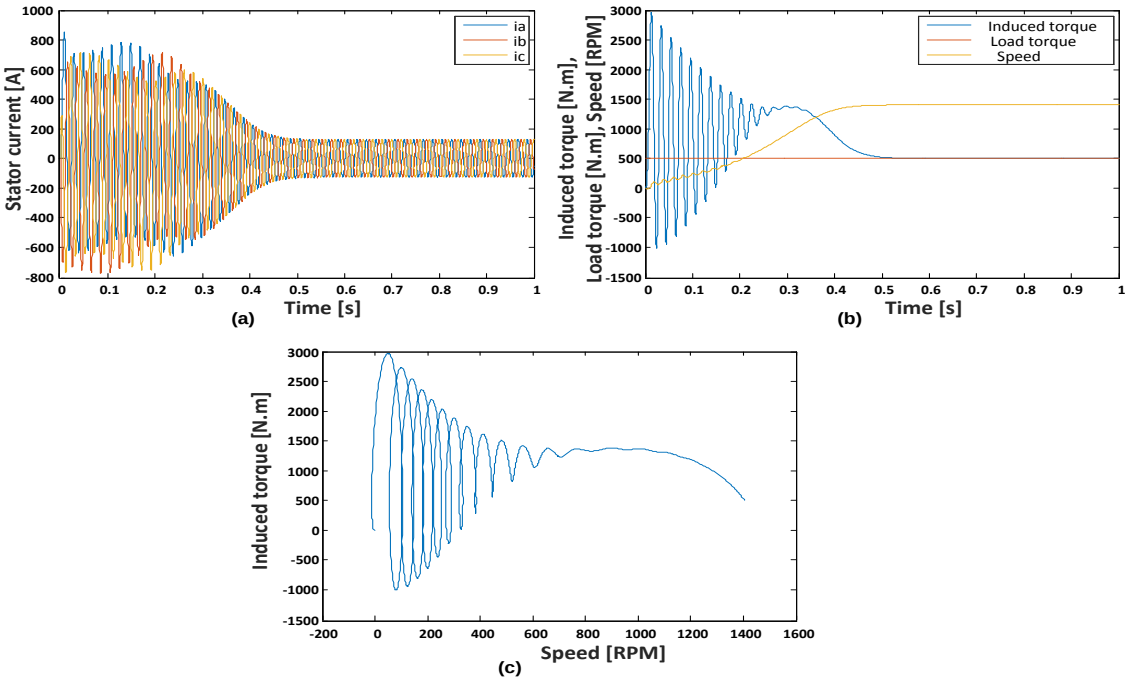

Fig. 21. a) Stator currents; b) speed, induced torque, and load torque; c) torque-speed characteristics.

5.2.2. *Star-Delta Starting*

Fig. 22 shows the simulation results of Star-Delta starting at a constant load.

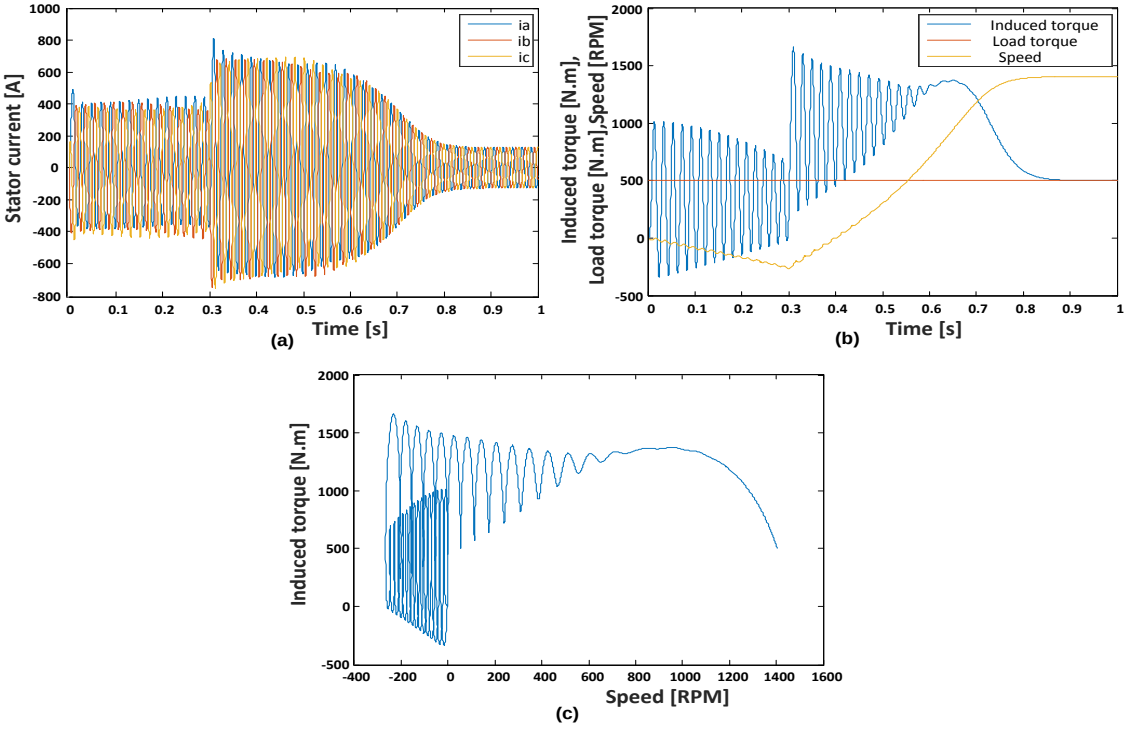

Fig. 22. a) Stator currents; b) speed, induced torque, and load torque; c) torque-speed characteristics.

5.2.3. *Soft Starting*

Fig. 23 shows the simulation results of soft starting at a constant load with an initial firing angle = 90° and slope = -180°.

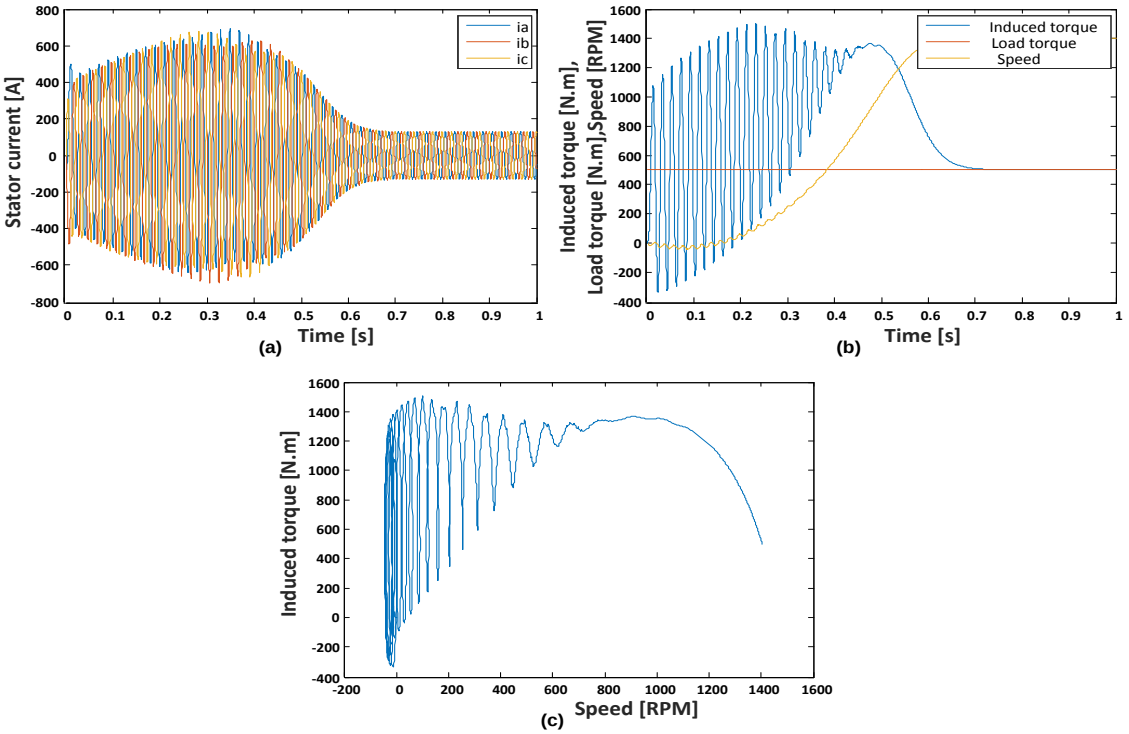

Fig. 23. a) Stator currents; b) speed, induced torque, and load torque; c) torque-speed characteristics.

5.3. Step Load

When the motor is starting at no-load and a load is then applied, the motor reaches the steady state at time after 0.72 s.

5.3.1. Direct On-line Starting

Fig. 24 illustrates the simulation results of an induction motor with a step load using direct on-line starting, where the motor reaches the steady state after 0.28 s.

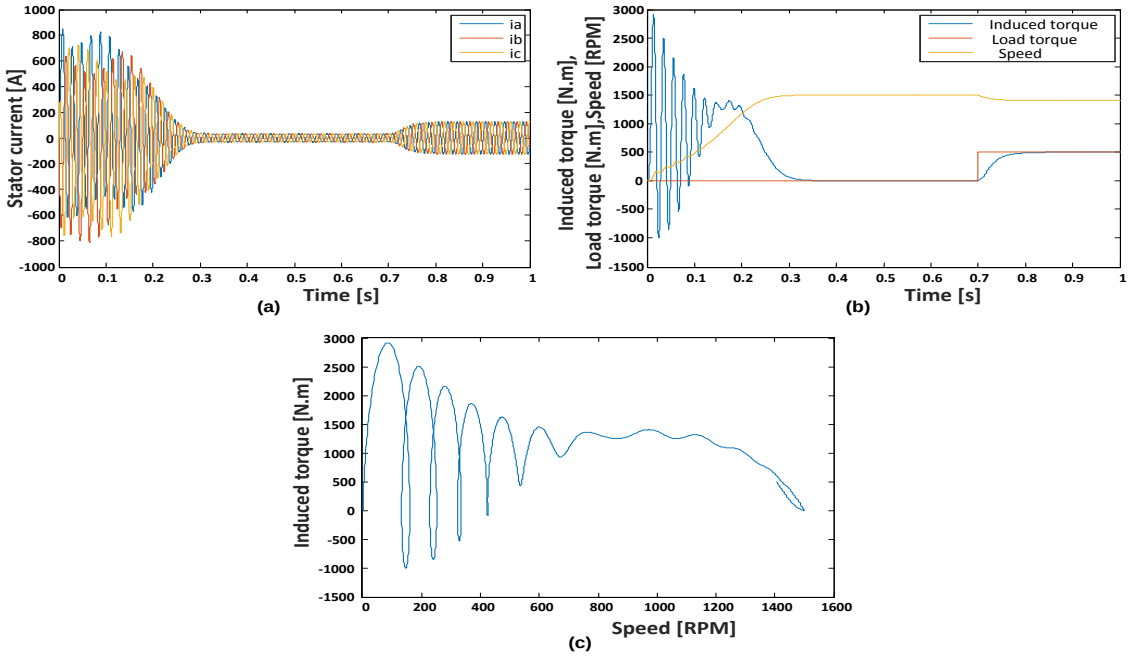

Fig. 24. a) Stator currents; b) speed, induced torque and load torque; c) torque-speed characteristics.

5.3.2. Star-Delta Starting

Fig. 25 shows the simulation results of an induction motor with a step load using Y/Δ starting, where the motor reaches the steady state after 0.45 s.

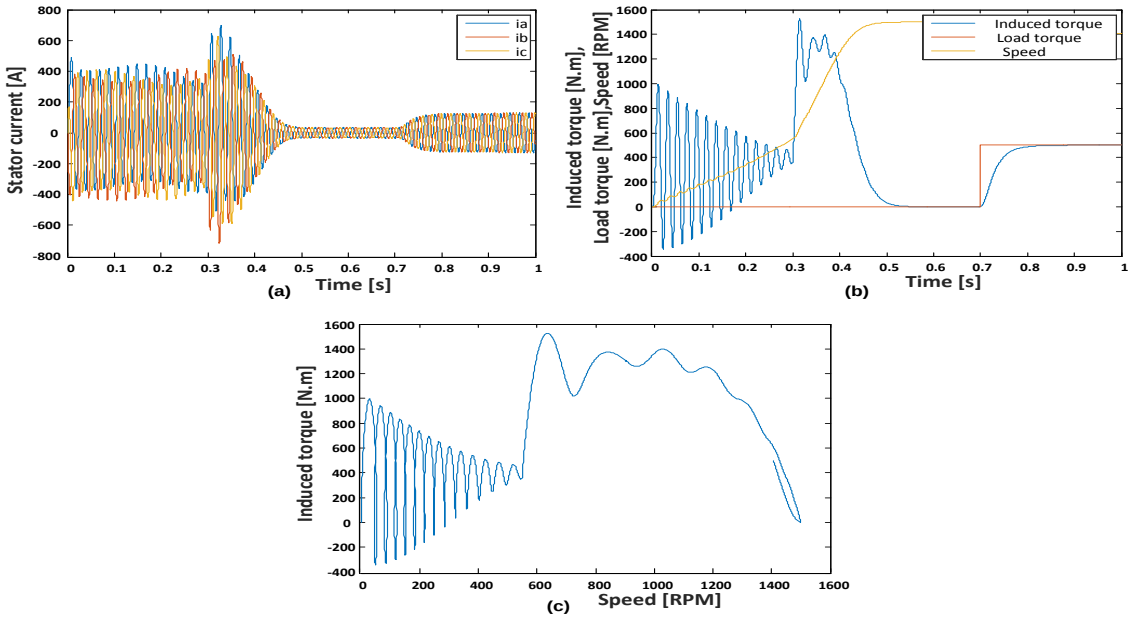

Fig. 25. a) Stator currents; b) speed, induced torque and load torque; c) torque-speed characteristics.

5.3.3. Soft Starting with zero Initial Firing Angle

Fig. 26 shows the simulation results of an induction motor using soft starting with a -120° slope and zero firing angle. The motor reaches the steady state after 1.35 s.

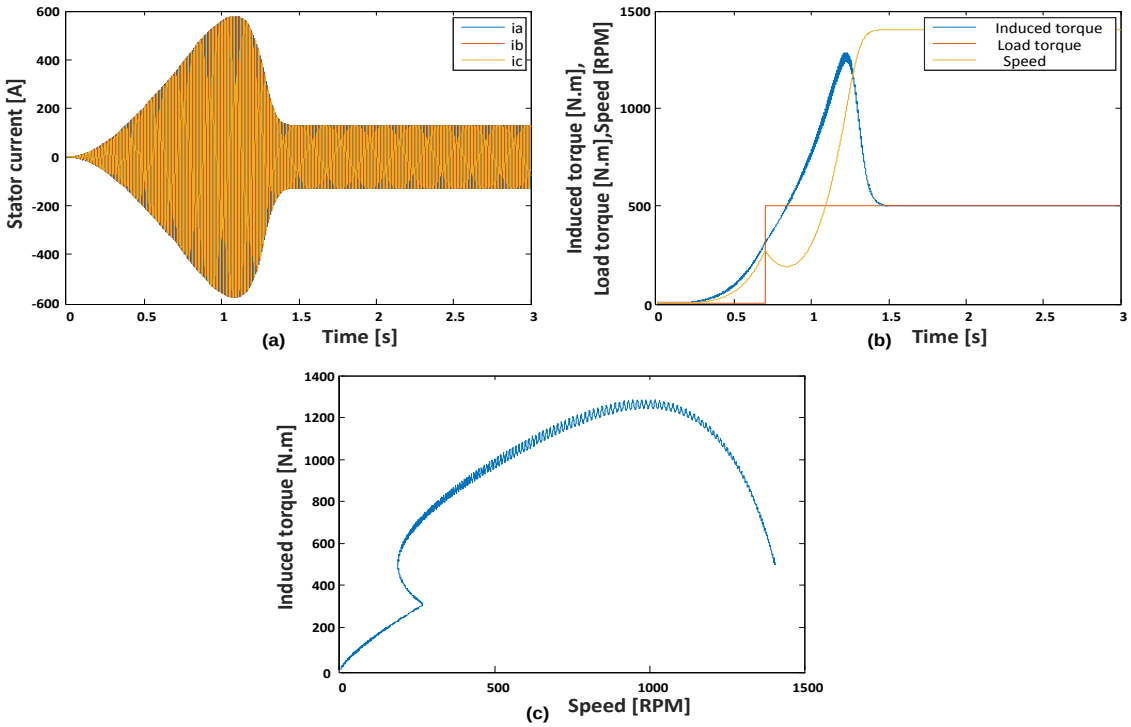

Fig. 26. a) Stator currents; b) speed, induced torque, and load torque; c) torque-speed characteristics.

Fig. 27 shows the simulation results of an induction motor using soft starting with a -180° slope and zero firing angle. The motor reaches the steady state after 0.75 s.

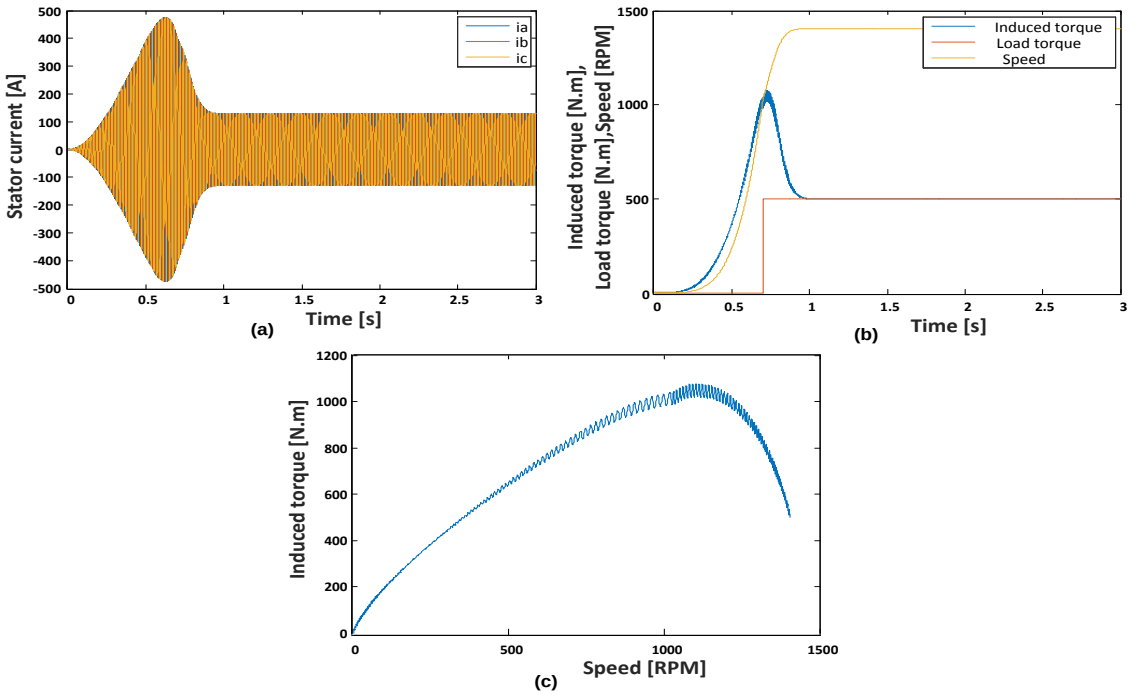

Fig. 27. a) Stator currents; b) speed, induced torque, and load torque; c) torque-speed characteristics.

Fig. 28 clarifies the simulation results of an induction motor using soft starting with a -360° slope and zero firing angle. The motor reaches the steady state after 0.52 s.

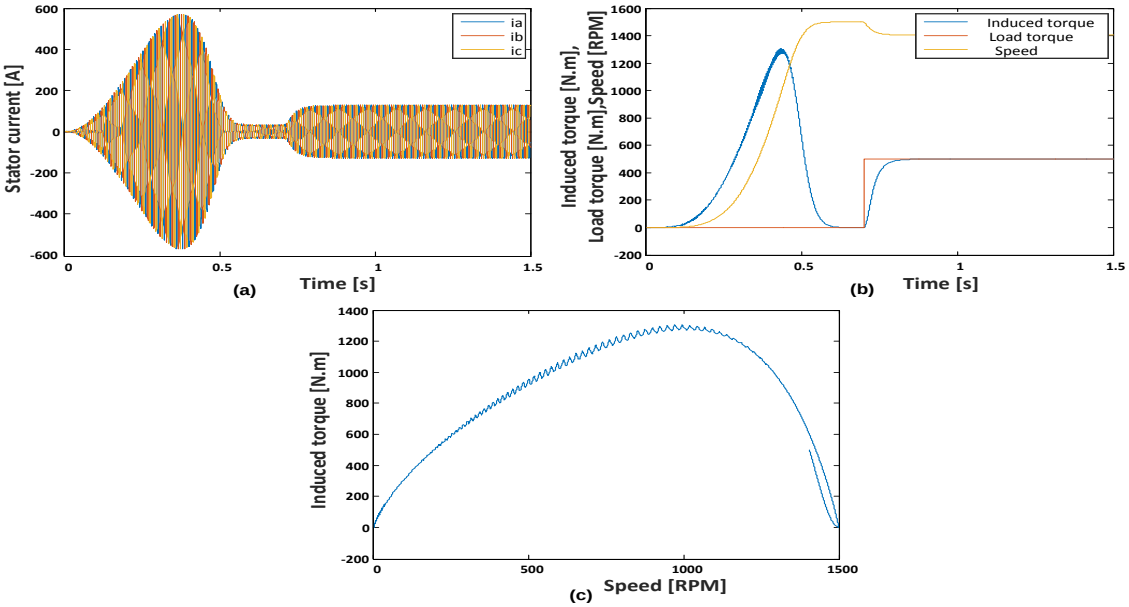

Fig. 28. a) stator currents; b) speed, induced torque, and load torque; c) torque-speed characteristics.

5.4. Ramp Load

In this case, the motor is starting with a ramp load, which is smoothly increased to reach the rated value after 1 s.

5.4.1. Direct On-line Starting

Fig. 29 illustrates the simulation results when the motor is started directly on-line with a ramp load, where the motor reaches the steady state after 0.28 s.

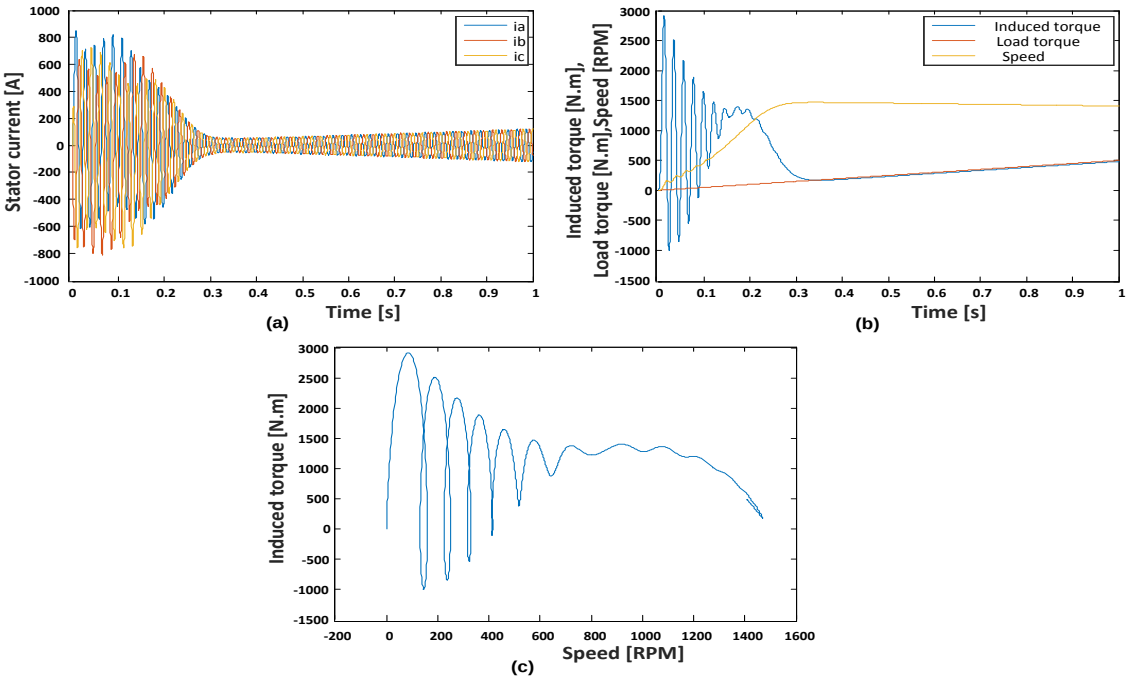

Fig. 29. a) Stator currents; b) speed, induced torque, and load torque; c) torque-speed characteristics.

5.4.2. *Star-Delta Starting*

Fig. 30 shows the simulation results when the motor is started using the star-delta method with a ramp load, where the motor reaches the steady state after 0.45 s.

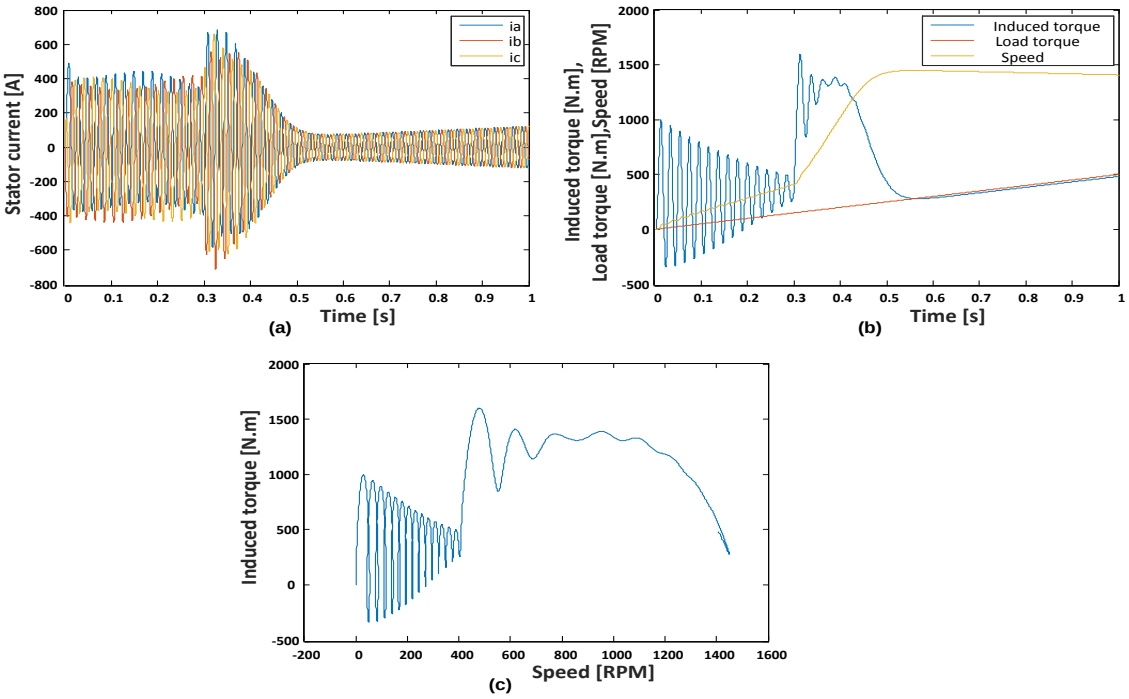

Fig. 30. a) Stator currents; b) speed, induced torque, and load torque; c) torque-speed characteristics.

5.4.3. *Soft Starting*

Fig. 31 shows the simulation results when the motor is started using soft starting with an initial firing angle of 90° and a Slope of -90° and a ramp load, where the steady state is reached after 0.5 s.

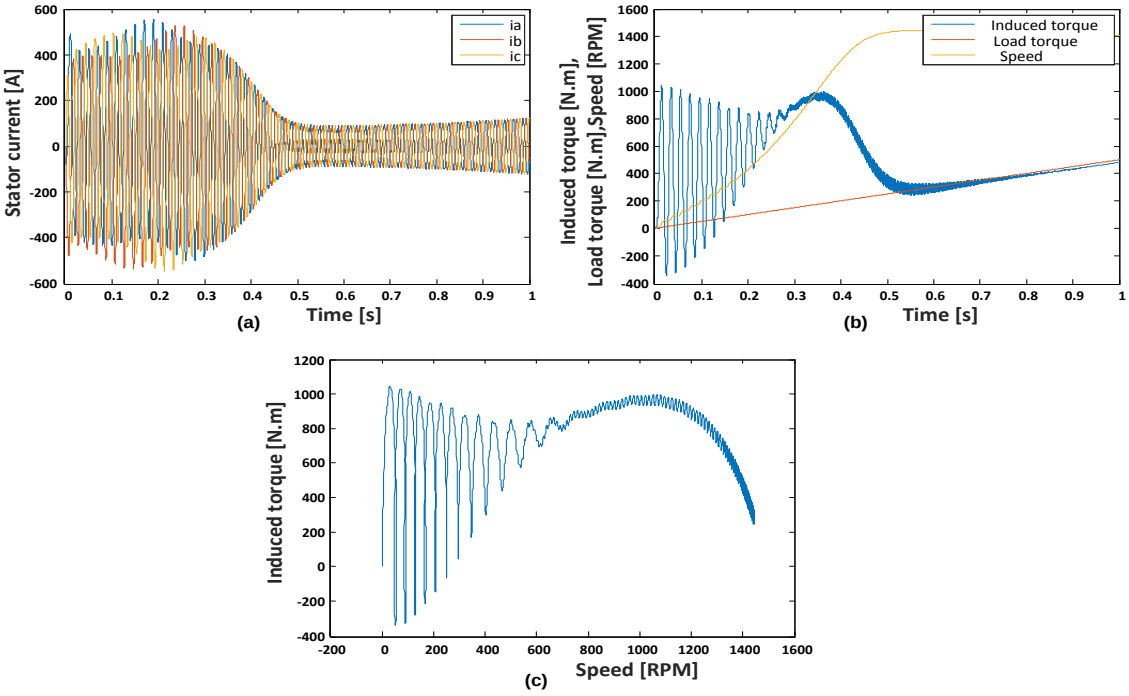

Fig. 31. a) Stator currents; b) speed, induced torque, and load torque; c) torque-speed characteristics.

Fig. 32 shows the soft starting results with an initial firing angle of 180° and a slope of -180° and a ramp load, where the steady state is reached after 1.15 s.

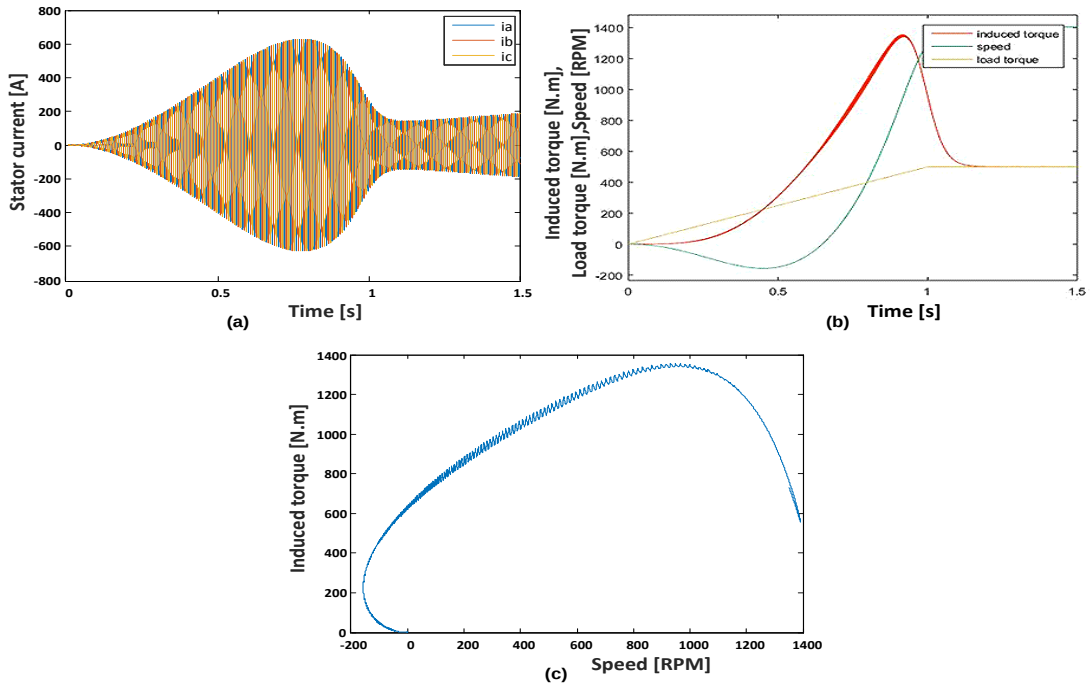

Fig. 32. a) Stator currents; b) speed, induced torque, and load torque; c) torque-speed characteristics.

6. CONCLUSIONS

In the current work a mathematical model for a three-phase induction motor was developed using d-q axis theory. Direct on-line starting, star-delta starting and soft starting of 3-phase induction motor were studied and analyzed. In soft-starting; the initial firing angle, the firing angle slope, and the load type were taken into account. The results showed that smooth acceleration reduced the stress on the electrical supply due to high starting currents. Shocks on the driven load due to a high starting torque are also reduced. At direct on-line starting these shocks reached a peak of about 14 PU during one cycle. In addition, the soft starting provided enough torque to accelerate the load while minimizing both mechanical and electrical shocks on the system and it gave acceptable starting time. The soft starting method provided about 0.5 second starting time duration for a 50-hp motor. Soft starting was proved to have the lowest current magnitude, thus eliminating shaft-torque pulsations during the starting process and ensuring smooth build-up of torque and speed. It was also clear that increasing the firing angle caused torque and current magnitude to increase faster, but it also caused the motor to reach the steady-state faster. The firing angle slope can be manipulated in order to avoid the motor loading before its induced torque reaches its load torque. When applying a step load, it was found crucial to pinpoint exactly the time at which the motor will be loaded. So, we either control the moment at which the motor will be loaded or manipulate the firing angle slope to avoid loading the motor before its induced torque reaches its load torque.

REFERENCES

[1] A. Bellure, M. Aspalli, "Dynamic d-q model of induction motor using simulink," *International Journal of Engineering Trends and Technology*, vol. 24, no. 5, pp. 252-257, 2015.

[2] S. Shah, A. Rashid, M. Bhatti, "Direct quadrate (d-q) modeling of 3-phase induction motor using matlab/simulink," *Canadian Journal on Electrical and Electronics Engineering*, vol. 3, no. 5, pp. 237-243, 2012.

[3] O. Barbarawi, A. Al-Rawashdeh, G. Qaryouti, "Simulink modelling of the transient cases of three phase induction motors," *International Journal of Electrical and Computer Sciences,* vol. 17, no. 04, pp. 6-15, 2018.

[4] O. Momoh, "Dynamic simulation of squirrel cage induction machine- a simplified and modular approach," *International Journal of Engineering Research and Technology*, vol. 2, no. 11, pp. 2307-2313, 2013.

[5] M. Salahat, O. Barbarawe, M. AbuZalata, S. Asad, "Modular approach for investigation of the dynamic behavior of three-phase induction machine at load variation," *Engineering*, vol. 3, pp. 525-531, 2011.

[6] K. Sandhu, V. Pahwa, "Simulation study of three phase induction motor with variations in moment of inertia," *ARPN Journal of Engineering and Applied Sciences*, vol. 4, no. 6, pp. 72-77, 2009.

[7] A. Eltamaly, A. Alolah, R. Hamouda, "Performance evaluation of three phase induction motor under different ac voltage control strategies' Part I'," *2007 International Aegean Conference on Electrical Machines and Power Electronics*, pp. 770-774, 2007.

[8] S. Ganar, O. Jodh, G. Gulhane, "Implementation of soft starter using 3 phase induction motor," *International Journal of Science and Research*, 2017.

[9] I. Boldea, S. Nasar, *Electric Drives*, Florida: CRC Press, 1998.

[10] C. Obeta, C. Mgbachi, I. Udeh, "Soft starter an alternative to motor control," *IJSAR Journal of Engineering and Computing,* vol. 2, no. 1, pp. 9-16, 2015.

[11] T. Wildi, *Electrical Machines, Drives, and power systems*, Pearson, 5th edition, 2014.

[12] A. Trzyadlowski, *Control of Induction Motors*, Salt Lake City: Academic press Co., 2001.

[13] C. Naxnin, Z. Qingfan, *The application of the fuzzy control technology in intelligent soft start*, PhD Thesis, Shandong University, 2012.

[14] A. Sharma, "Simulation of three phase soft starter using multiple SCRs," *International Journal of Engineering Trends and Technology*, vol. 49, no. 7, pp. 451-456, 2017.

[15] B. Trivedi, J. Raval, J. Desai, K. Sonwane, "Soft start of induction motor using TRIAC switching," *International Journal of Engineering Development and Research*, vol. 5, no. 2, pp. 1635-1639, 2017.

[16] S. Akshaykumar, T. Sagar, S. Vijay, P. Mone, "Soft starting of three phase induction motor," *International Journal for Research Trends and Innovation*, vol. 2, no. 5, pp. 1-2, 2017.

[17] A. Menaem, A. Amin, "A proposed soft starting technique for three-phase induction motor using ANN," *16-th International Middle-East Power Systems Conference*, 2014.